Atmospheric
Measurement
Techniques
Discussions

Open Access

Inversion of droplet aerosol analyzer data for long-term aerosol-cloud interaction measurements

M. I. A. Berghof[1], G. P. Frank[1], S. Sjogren[1,*], and B. G. Martinsson[1]

[1]Division of Nuclear Physics, Lund University, Lund, Sweden
[*]now at: University of Applied Sciences Northwestern Switzerland, Brugg-Windisch, Switzerland

Correspondence to: M. I. A. Berghof (maria.berghof@pixe.lth.se)

Discussion Paper | Discussion Paper | Discussion Paper | Discussion Paper |

AMTD

6, 10269–10295, 2013

Inversion of DAA data for longterm AIC measurements

M. I. A. Berghof et al.

Title Page

Abstract	Introduction
Conclusions	References
Tables	Figures

|◄ | ►|
◄ | ►
Back | Close

Full Screen / Esc

Printer-friendly Version

Interactive Discussion

Abstract

The droplet aerosol analyzer (DAA) was developed to study the influence of aerosol properties on clouds. It measures the ambient particle size of individual droplets and interstitial particles, the size of the dry (residual) particles after the evaporation of water,
5   and the number concentration of the dry (residual) particles. A method was developed for the evaluation of DAA data to obtain the three-parameter dataset: ambient particle diameter, dry (residual) particle diameter and number concentration. First results from in-cloud measurements performed on the summit of Mt. Brocken in Germany are presented. Various aspects of the cloud aerosol dataset are presented, such as the
10 number concentration of interstitial particles and cloud droplets, the dry residue particle size distribution, droplet size distributions, scavenging ratios due to cloud droplet formation and size-dependent solute concentrations. This dataset makes it possible to study clouds and the influence of the aerosol population on clouds.

1   Introduction

15 Clouds affect the Earth's climate in a number of ways, for example they regulate the hydrological cycle and redistribute energy via the transport of water vapor and latent heat in the atmosphere. Many factors influence the macrophysics and microphysics of clouds. The macrophysics of clouds is affected by large-scale meteorological conditions such as updraft velocity, turbulent mixing or atmospheric layering. Cloud droplets
20 form by the condensation of water vapor on aerosol particles. As a consequence, the microphysical conditions are influenced by the macrophysics, the particle number concentration and size distribution, the chemical composition, and the mixing state of the atmospheric aerosol. The first (Twomey) indirect aerosol effect describes changes in cloud properties induced by changes in the properties of aerosol particles (Warner,
25 1968; Twomey, 1974; Albrecht, 1989; Liou and Ou, 1989; Lohmann and Feichter, 2005). It is still being debated whether changes in the microphysical properties of

Title Page

Abstract | Introduction

Conclusions | References

Tables | Figures

Back | Close

Full Screen / Esc

Printer-friendly Version

Interactive Discussion

clouds also influence the amount of clouds and liquid water content. These changes are also associated with changes in precipitation efficiency and thus cloud lifetime (second indirect aerosol effect, Albrecht, 1989; Stevens and Feingold, 2009).

Different instruments can be used to determine the properties of atmospheric aerosols and clouds, leading to an improved understanding of their interaction. A differential mobility particle spectrometer (DMPS) can be used to measure the size distribution in the range between a few nm up to several hundred nm, allowing the interstitial aerosol or the (dry) aerosol size distribution to be monitored, while an optical particle counter (OPC) can be used to measure the size of cloud droplets. An OPC measures the amount of light scattered by each particle, from which the concentration and size of particles can be determined (Sorensen et al., 2011). The ground-based fog monitor is an optical spectrometer that samples fog and cloud droplets in the size range between 2 and 50 µm (FM-120, Spiegel et al., 2012), and can be used to evaluate super-cooled droplets, which is an advantage over DMPS and OPC. All three instruments can provide information on the dry aerosol particle and ambient droplet size distribution over a large size range, but even with the combined use of these methods it is not possible to obtain information on the relation between the dry residue particle size and ambient droplet size.

A counterflow virtual impactor uses inertial separation to divide the ambient particle size distribution at a cut-off diameter into distributions for droplets and interstitial aerosol particles with trace gases. The cut-off diameter can be set between 1 and 30 µm (Anderson et al., 1993; Noone et al., 1988; Ogren et al., 1985). The collected droplets and interstitial aerosol can then be analyzed chemically or their dry (residual) particle size distribution can be determined using other instruments (Slowik et al., 2011). Although the droplets can be collected, it is not possible to relate droplet size to residue particle size.

This relation and both the dry aerosol size distribution in the range between 50 and 750 nm and the ambient aerosol distribution in the range between 0.1 and 25 µm can be obtained using the droplet aerosol analyzer (DAA, Martinsson, 1996). This

M. I. A. Berghof et al.

instrument was especially developed to study the interaction between aerosol particles and cloud/fog droplets. The DAA measures the ambient size of individual droplets and interstitial particles, the size of the dry (residual) particles after the evaporation of water vapor, and the number concentration. This gives a unique three-parameter dataset (ambient particle diameter, dry (residual) particle diameter, and number concentration), making it possible to study the interaction between atmospheric aerosol properties and cloud properties in detail (Martinsson et al., 1999).

The ability of the DAA to give very detailed information on cloud microphysics, and the aerosol-cloud droplet relation has been demonstrated in previous field campaigns. The DAA has been used to study the formation of clouds on a mountain ridge in north-western England, UK (Martinsson et al., 1999, 1997; Cederfelt et al., 1997) and in north-eastern Tenerife (Martinsson et al., 2000), as well as fog/cloud formation in the Po Valley in northern Italy (Frank et al., 1998). When studying fog formation in the Po Valley it was shown by Frank et al. (1998) that droplet activation does not occur at a fixed diameter, as the observed fogs showed a continuous droplet size distribution. The results were reproduced by a parcel model, showing that in highly polluted regions with a low rate of temperature change during fog formation, fog may consist of only unactivated droplets.

A closure study conducted by Martinsson et al. (2000) on the number concentration obtained from the DAA and a DMPS placed upstream and in-cloud showed overall good agreement; 43 out of 49 measurements (88 %) fulfilled the criteria for closure. Good agreement has also been found when comparing the cloud droplet number concentration obtained with the DAA measurements that passed the closure test with a forward scattering spectrometer probe (FSSP) for concentrations below 1000 cm^{-3}. For higher cloud droplet concentrations the FSSP gave significantly lower values due to saturation effects in the FSSP (Martinsson et al., 2000).

A new version of the DAA with better time resolution (10 min) designed especially for long-term measurements was developed and was used for in-cloud measurements on the peak of Mt. Brocken (Germany) in 2010. The previous manual evaluation of

large amounts of data was very time consuming, and therefore an inversion algorithm, presented in this paper, was developed to evaluate long term measurements by a more automated data processing.

2 The DAA instrument

A schematic of the DAA is shown in Fig. 1. The instrument is described in more detail by Frank et al. (2013). It consists of an outdoor and an indoor part. Cloud droplets and interstitial particles are collected in the outdoor part through an inlet directed towards the wind. To achieve a well defined charge state, the aerosol is first passed through a bipolar charger (BiCh) and the a unipolar charger (UniCh), where the droplets acquire a charge level dependent on their size, while still at ambient conditions Frank et al., 2004). Water is removed in the dryer, described in Sjogren et al. (2013), and the dry aerosol then enters the indoor part.

At this stage the charge level of the particles is related to their ambient size. The particles are selected according to their electrical mobility in the first differential mobility analyzers (DMA 1a and 1b). The following combination of Bipolar Charger (BiCh), DMA and Condensation Particle Counter (CPC) gives the electrical mobility of the singly charged droplet residuals for a given dry diameter. Once the dry particle diameter and the electric mobility of the residual particles are known, their charge state can be calculated, which is then related to the ambient particle diameter via the calibration of the unipolar charger.

During operation of the DAA, the voltage of the DMAs 2a–f is fixed, while the voltage of DMA 1a and 1b is varied over different charge levels from the unipolar charger. The mobility step between each DMA 2a–f is set to two. The mobility step in DMA 1a and 1b is set to $\sqrt{2}$ so as to coincide with the DMA 2 mobility of singly, doubly, quadruply, etc., charged particles from the unipolar charger. This allows for efficient detection of small particles, carrying few elementary charges. From each DMA 1a and 1b voltage a set of six measurements from DMA 2a–f are obtained.

3 DAA data evaluation

An inversion technique was applied to the DAA raw data to obtain the three-parameter dataset consisting of ambient particle diameter, dry (residual) particle diameter and number concentration. The basic variables were first calculated from the corrected raw data, resulting in the charge distribution caused by the unipolar charger (Fig. 1) for every dry particle diameter measured. Based on the calibration of the unipolar charger, a function can be derived to describe the relation between charge distribution and ambient particle size. In the second step of the data evaluation this function is used to extract the ambient particle diameter, D_d, and concentration, N_{UCh}, of particles and droplets entering the DAA, corresponding to each charge distribution and thus to each dry (residual) particle diameter, D_p. The DAA three-parameter dataset then consists of the ambient particle diameter, D_d, the dry (residual) particle diameter, D_p, and the number concentration, N_{UCh}, in each dry particle interval measured.

3.1 Raw data

During one measurement run the voltage of DMA 1a and 1b is stepped over different charge levels, while the voltage of DMA 2a–f is fixed. As the transport times in the instrument is known, it is possible to select steady-state data and to achieve a time resolution of 10 min for one complete measurement.

Two measurement runs are made at two different voltages of DMA 2a–f. The first run at voltages representing small diameters (59 to 545 nm) and the second run is decreased by a factor of $\sqrt{2}$ in terms of electrical mobility, Z_p, to increase the resolution in dry particle diameter (75 to 776 nm). Both runs can be used independently, giving a time resolution of 10 min, and a time resolution of 20 min with full size resolution.

The DAA raw data from each run consist of CPC raw counts, N_{counts}, the CPC counting time, t_{count}, the High Voltage of DMA 1a and 1b and DMA 2a–f, U, the sheath air flow, Q_{sh}, and the aerosol flow, Q_{ae}, for each DMA, as well as atmospheric pressure, p, and aerosol temperature T_{ae}. The dry particle diameter D_p, electrical mobility, Z_p,

electrical charge level, q_{DAA}, and the raw number concentration, N_{raw}, can be calculated from this dataset.

3.2 Data correction

The DAA raw concentration is corrected for losses that occur after the second bipolar charger (losses in DMA 2a–f). Corrections are also made for particle losses in DMA 1a and 1b that occur upstreams of the bipolar charger. The loss-corrected concentration data are then corrected for multiple charging in the second bipolar charger.

3.2.1 DMA correction

A perfect DMA can be described by an ideal, symmetric transfer function, which is triangular. Imperfections in the DMA may result in broadening of the transfer function and losses of particles (Martinsson et al., 2001). Further losses and broadening due to Brownian diffusion can cause the transfer function to be dependent on particle size (Stolzenburg, 1988). Two parameters are used to characterize the imperfections of the DMAs. A broadening factor, μ (≤ 1), describes the width of the transfer function leading to a broader individual transfer function while conserving its area. Particle loss is described by a loss factor, λ (≤ 1), leading to a decrease in area while conserving its width. Both parameters are specific to each DMA and were determined experimentally for 230 nm particles, as described in Martinsson et al. (2001). The size dependence of both parameters was estimated as described in Karlsson and Martinsson (2003). The resulting parameters were averaged for each DMA over both DAA runs, leading to an error of less than 0.5 % due to the size dependence of Brownian diffusion. The estimates for the eight DMAs are in the range $\mu = 0.87$ to 1.00 and $\lambda = 0.81$ to 1.00. Both DMA loss and broadening are accounted for in each charge distribution before the bipolar charge correction.

Another feature of the instrument is the size range covered by each of the DMA 2a–f. During a run the voltage of DMA 2a–f is kept constant and the mobility step between

each of the DMA 2a–f is set to two. In order to quantify the mobility distribution each DMA measurement must be converted to represent the DMA stepping factor used as described by Cederfelt et al. (1997).

3.2.2 Bipolar charger correction

The ambient particles and droplets entering the DAA are charged, then dried and selected according to charge level in DMA 1a and 1b. Before entering the second series of DMAs, the particles selected by DMA 1a and 1b are multiply charged in a bipolar charger.

In order to correct for multiple charging, it was assumed that the influence of multiply charged particles larger than the largest particle size measured in each run could be neglected. This is approximately valid for size distributions showing a rapid decrease in number concentration with increasing size, which is usually the case for atmospheric aerosol at the maximum sizes in the two different DMA runs (593 and 751 nm). Doubly and quadruply charged particles with a dry particle diameter measured by a certain DMA 2a–f will have a higher mobility. These will be detected by the DMA 2a–f measuring the closest and second closest smaller dry particle diameter. Their fraction were calculated based on the charge distribution described in Wiedensohler (1988).

To be able to correct for triply charged particles, a linear relation was assumed between the concentration of triply charged particles and the concentration of doubly and quadruply charged particles. The fraction of triply charged particles, $f(D_P, -3)$, can thus be included in the fraction of doubly, $f(D_P, -2)$, and quadruply, $f(D_P, -4)$, charged particles:

$$f^*_{D_P,-2} = f_{D_P,-2} + \frac{1}{2} f_{D_P,-3} \tag{1}$$

$$f^*_{D_P,-4} = f_{D_P,-4} + \frac{1}{2} f_{D_P,-3} \tag{2}$$

Inversion of DAA data for longterm AIC measurements

M. I. A. Berghof et al.

Title Page

Abstract	Introduction
Conclusions	References
Tables	Figures

Back | Close

Full Screen / Esc

Printer-friendly Version

Interactive Discussion

The charge distribution measured in each of the DMA 2a–f is thus corrected by subtracting the determined amount of doubly and quadruply charged particles from the other DMA 2a–f channels.

Finally, the concentration is corrected to standard laboratory pressure (1013.25 hPa) and temperature (293.15 K) giving the charge distribution measured by the DAA, $N^{DAA}(q_{DAA})$.

3.3 DAA inversion algorithm

After applying the above described corrections, we obtained the corrected charge distribution of the ambient aerosol as measured by the DAA. Figure 2 shows the DAA data obtained during one run for each of the DMA 2a–f with its corresponding dry particle diameter, D_p. For small charge levels (i.e. small ambient particles), singly and doubly charged particles can be observed, whereas particles with two consecutive charge levels cannot be resolved higher up in the spectrum. In the next step, a function is fitted to the data, as shown in Fig. 2. The function fitted is the resulting charge distribution of droplets of a certain ambient particle diameter D_d passing through the DAA system, using the ambient particle diameter, D_d, and the number concentration of particles entering the unipolar charger, N_{UCh}, as fitting variables. The following section describes how this function is obtained by first calculating the charge distribution downstream of the unipolar charger, and then the charge distribution downstream of DMA 1a and 1b and DMA 2a–f.

3.3.1 Unipolar charger

When the aerosol enters the DAA it first passes through a bipolar charger to achieve a well defined charge state. By passing the unipolar charging unit the aerosol acquires positive charges depending on their particle diameter. The resulting charge distribution thus depends on the ambient size of the particles entering the DAA. The relation between the arithmetic mean charge level and the mean ambient particle diameter in μm

Inversion of DAA data for longterm AIC measurements

M. I. A. Berghof et al.

Title Page

Abstract	Introduction
Conclusions	References
Tables	Figures

Back | Close

Full Screen / Esc

Printer-friendly Version

Interactive Discussion

was calibrated in the size range 0.12 to 17 µm by Frank et al. (2004), and was used here:

$$D_{\mathrm{d}}(q_{\mathrm{a}}) = -2.394 + (3.103 + 0.377 \cdot q_{\mathrm{a}})^{0.771}. \tag{3}$$

Only particles becoming positively charged by the unipolar charger will be detected in the system. To determine the ambient particle size and concentration, the fraction of singly and doubly charged particles must be detectable. This may not be the case for ambient particles with small diameters at low concentrations, since the fraction of detected doubly charged particles may be too small. This leads to an error when determining the ambient particle size. For ambient particles with a size of $D_{\mathrm{p}} = 50$ nm the error in ambient size is 10 % for a concentration of $\mathrm{d}N/\mathrm{d}\log D_{\mathrm{p}} = 12.5$ cm^{-3}.

Large particles can be lost in the DAA inlet, thus the upper limit was set to 25 µm. The calibration range is therefore somewhat smaller than the measurement range. The calibration range was extrapolated by Frank et al. (2004) based on the charging model presented by Lawless (1996).

An α-source, Cm-244, was used to charge particles passing through the unipolar charger. Since the half-life of this source is 18.1 yr, the calibration performed by Frank et al. (2004) may have changed, since radioactive decay would have resulted in a decrease in the number of charges for a certain droplet size. Therefore, the ambient particle diameter used here may be slightly underestimated. However, this will not affect the main subject of this paper.

3.3.2 Charge distribution downstream of the unipolar charger

The shape of the charge distribution downstream of the unipolar charger depends on the ambient particle size, D_{d}, of the entering particles. Calibrations show that the charge distribution downstream of the unipolar charger for particles smaller than 0.61 µm follows a normal distribution, whereas for particles larger than 3.15 µm it follows a log-normal distribution. Between these limits a linear combination of both distributions was used.

Ambient particles and droplets smaller than 0.61 µm acquire an arithmetic mean charge below $q_a = 2.82$. Their resulting charge distribution downstream of the unipolar charger follows a normal distribution:

$$\frac{dN^{\text{Charger}}_{[<0.61\,\mu m]}(q_i)}{dq_i} = \frac{N_{\text{UCh}}}{\sqrt{2\pi}\sigma_a} \exp\left(-\frac{1}{2}\left(\frac{q_i - q_a}{\sigma_a}\right)^2\right) \qquad (4)$$

for integer charge-bins q_i and an arithmetic mean charge of q_a and standard deviation σ_a

$$q_a = \frac{(D_d[\mu m] + 2.394)^{\frac{1}{0.771}} - 3.103}{0.377} \qquad (5)$$

$$\sigma_a = \sqrt{0.28 + 1.51 q_a}. \qquad (6)$$

Ambient particles and droplets larger than 3.15 µm acquire an arithmetic mean charge greater than $q_a = 16.23$. Their resulting charge distribution downstream of the unipolar charger follows a log-normal distribution (Frank et al., 2004):

$$\frac{dN^{\text{Charger}}_{[>3.15\,\mu m]}(q_i)}{d\log q_i} = \frac{N_{\text{UCh}}}{\sqrt{2\pi}\log(\sigma_g)} \exp\left(-\frac{\log^2\left(\frac{q_i}{q_g}\right)}{2\log^2(\sigma_g)}\right) \qquad (7)$$

for integer charge bins q_i and a geometric mean charge of q_g and standard deviation σ_g:

$$q_g = \frac{q_a}{\exp\left(\frac{\log^2(\sigma_g)}{2}\right)} \qquad (8)$$

$$\sigma_g = 1.99 - 0.027 D_d \qquad (9)$$

with D_d in µm.

In the size range 0.61–3.15 µm, ambient particles and droplets acquire an arithmetic mean charge of $q_a = 2.82$ to 16.23. Here, a combination of normal and log-normal distributions was used:

$$N_{[0.61-3.15\,\mu m]}^{Charger}(q_i) =$$

$$(1 - \xi(q_i)) \times dq_i \times \left(\frac{N_{UCh}}{\sqrt{2\pi}\sigma_a} \exp\left(-\frac{1}{2}\left(\frac{q_i - q_a}{\sigma_a}\right)^2 \right) \right)$$

$$+ \xi(q_i) \times d\log q_i \times \left(\frac{N_{UCh}}{\sqrt{2\pi}\log(\sigma_g)} \exp\left(-\frac{\log^2\left(\frac{q_i}{q_g}\right)}{2\log^2(\sigma_g)} \right) \right) \tag{10}$$

for integer charge bins q_i and the linearly increasing factor $\xi(q_i)$:

$$\xi(q_i) = \begin{cases} 0, & q_i \leq 2.82 \\ (q_i - 2.82)/(16.23 - 2.82), & 2.82 < q_i < 16.23 \\ 1, & q_i \geq 16.23 \end{cases} \tag{11}$$

The resulting charge distribution downstream of the unipolar charger is used to calculate the charge distribution downstream of both series of DMAs, as described below.

3.3.3 Charge distribution downstream of the DMAs

The charged droplets downstream of the unipolar charger are dried and passed through DMA 1a and1b and one of the second series of DMAs (2a–f). The calculated charge distribution downstream of the DMAs, f_{fit}, is then compared with the measured DAA charge distribution.

It is important to know the individual transfer functions of each of the DMAs in order to estimate the charge distribution downstream of the DMAs. Due to the width of the

Inversion of DAA data for longterm AIC measurements

M. I. A. Berghof et al.

Title Page

Abstract | Introduction

Conclusions | References

Tables | Figures

◀ | ▶

◀ | ▶

Back | Close

Full Screen / Esc

Printer-friendly Version

Interactive Discussion

DMA transfer function when measuring a certain charge, q_{set}, particles within a certain charge range $[q_{min}, q_{max}]$ will be selected. The fraction of particles with charges $q_i = 1, 2, \ldots, n$ measured in a certain charge bin, q_{DAA}, of the DAA can be calculated by convolution of the transfer function of DMA 1a or 1b and the corresponding of the DMA 2a–f. This fractions can be expressed in the transmission matrix, $\mathbf{T}$, for an ideal DMA with a flow ratio of $\frac{Q_{ae}}{Q_{sh}} = \frac{1}{4}$ it can be derived as (only part of the matrix is given):

$$q_{DAA} = \left(\sqrt{2}, 2, 2\sqrt{2}, 4 \right) \tag{12}$$

$$q_i = \left(1, 2, 3, 4, 5, 6, 7 \right) \tag{13}$$

$$\mathbf{T}(q_{DAA}, q_i) = \begin{pmatrix} (\sqrt{2}, 1) & \cdots \xrightarrow{q_i} & (\sqrt{2}, 7) \\ \vdots & q_{DAA} & \\ \downarrow & & \\ (4, 1) & & (4, 7) \end{pmatrix}$$

$$= \begin{pmatrix} 0.036 & 0.051 & 0 & 0 & 0 & 0 & 0 \\ 0 & 0.667 & 0.014 & 0 & 0 & 0 & 0 \\ 0 & 0.036 & 0.636 & 0.051 & 0 & 0 & 0 \\ 0 & 0 & 0.094 & 0.667 & 0.256 & 0.014 & 0 \end{pmatrix} \tag{14}$$

This example shows that around 66.7 % of the particles with a charge of $q_i = 2$ will appear in the DMA channel corresponding to charge $q_{DAA} = 2$, 5.1 % will appear in the DMA channel corresponding to charge $q_{DAA} = \sqrt{2}$, and 3.6 % in the DMA channel corresponding to charge $q_{DAA} = 2\sqrt{2}$.

The charge distribution downstream of the DMAs is the sum of the product of each row of the transmission matrix $\mathbf{T}$ and the charge distribution downstream of the unipolar charger $N^{Charger}(q_i)$

$$f_{fit}(q_{DAA}) = \sum_i \left(T(q_{DAA}, q_i) \times N^{Charger}(q_i) \right) \tag{15}$$

The function f_{fit} is the calculated charge distribution, assuming that N_{UCh} particles and droplets of ambient particle size D_d enter the unipolar charger. Values of the co-efficients N_{UCh} and D_d can be found by nonlinear least squares curve fitting of the fit function f_{fit} to the measured DAA data $N^{DAA}(q_{DAA})$. It is possible to use more than one size for the ambient particles and droplets.

Having determined the values for the variables N_{UCh} and D_d from the fit, it is possible to directly relate ambient particle diameter, dry (residual) particle diameter and number concentration.

3.3.4 Inlet correction

N_{UCh} is the concentration of particles entering the unipolar charger. In the last step of the data evaluation losses in the DAA inlet must be accounted for. A wind vane, which consists of an exchangeable cone followed by a 90° bend connected to the unipolar charger unit, directs the DAA inlet towards the wind. Three inlet cones are available, designed for isokinetic sampling at wind speeds of 2, 5 and $10\,\mathrm{m\,s^{-1}}$. Depending on the actual wind speed, certain ambient particle diameters may be over- or underrepresented in the sampled aerosol. To obtain the concentration, N, of particles entering the DAA inlet, the calculated concentration of particles entering the unipolar charger obtained from the fit, N_{UCh}, must be corrected. The correction depends on the isokinetic sampling speed of the inlet, the actual wind speed, and the ambient particle diameter of the aerosol particles, D_d, and was performed as described by Belyaev and Levin (1974).

3.4 Uncertainties

The DAA measures the number concentration, dry particle diameter and ambient particle diameter. The uncertainty in dry particle diameter is estimated to be 6 %, and is due to the uncertainties in the DMA high voltage (estimated to be 2 %), the sheath air flow (estimated to be 2 %) and the geometrical dimensions of the DMAs (inner and

outer radius and electrode length) (estimated to be 5 %). The uncertainty in ambient particle diameter is estimated to be 12 %, due to uncertainties in the DMA high voltage (estimated to be 2 %), the sheath air flow (estimated to be 2 %), the geometrical dimensions of the DMAs (estimated to be 5 %) and the calibration curve used for the unipolar charger (estimated to be 10 %). Additional uncertainty, at present not quantified, will arise from the decay of the radioactive source in the unipolar charger. The estimated uncertainty in the number concentration $dN/d\log D_p$ for each dry particle diameter obtained from the fitted function is below 13 % for ambient concentrations above $dN/d\log D_p = 50\,\mathrm{cm}^{-3}$. This is due to the uncertainties in the standard error for Poisson counting of the raw counts, the uncertainty in aerosol flow (regulated by a proportional-integral-derivative controler (PID), estimated to be 5 %), the correction for the mobility range covered (estimated to be 10 %), and the bipolar charge correction (estimated to be 5 %).

4 Results

After fitting the ambient size distribution for each of the six dry particle diameters measured, it is possible to calculate the ambient particle and dry particle size distributions and several other parameters, as described in this section.

4.1 The capability of the DAA

In 2010, the DAA was placed at the summit of Mt. Brocken in the Harz region of central Germany to perform in-cloud measurements. An event with stable cloud conditions (31 August 2010, 23:30 to 1 September, 01:30 UTC) was selected to demonstrate the capability of the DAA. The DAA relates directly ambient particle diameter, dry (residual) particle diameter and the number concentration, as for example shown in Fig. 3a. Interstitial particles (red) and droplets (blue) can be identified. The cloud droplets were between 6 and 13 µm in diameter, and formed on particles in the size range 86 to 546 nm.

The interstitial aerosol formed on dry (residual) particles in the size range from 50 to 300 nm, and had ambient particle diameters from 0.13 to 1.1 μm. The three black lines in the x–y plane indicate the critical diameter of activation according to Köhler's theory for different volume fractions of ammonium sulfate in the particles, $D^*_{V(AS)}$. For large dry particle size those lines can intersect the dropmode, this indicates that some of the cloud droplets might not have been activated according to Köhler's theory. Although the droplets formed on large dry particles might not be activated according to Köhler's theory, they would be larger than the activated droplets formed on smaller nuclei, and should be regarded as cloud droplets. Both ambient and dry (residual) size distributions can be derived by projecting the concentration onto the corresponding axis and dividing by $d\log D_p$ or $d\log D_d$ as explained below.

For the selected event, 48 h back trajectories from Mt. Brocken were derived with the HYSPLIT model (Draxler and Rolph, 2013), as shown in Fig. 3b. They show that the air arrived via southern Sweden and the Baltic Sea north-east of Mt. Brocken, a region with an annual fine matter average ($PM_{2.5}$) of less than 10 μg m^{-3} according to the European Environment Agency (2012). The air approached Mt. Brocken via north-eastern Germany from the north ($PM_{2.5}$ of 10 to 20 μg m^{-3}) with an average wind speed of 10 m s^{-1} and ambient temperature of 5 °C, measured at the measurement station on summit of Mt. Brocken.

The total number concentration of dry (residual) particles from cloud droplets and interstitial particles in the dry particle size range 49 to 563 nm during the event was stable at 515 ± 50 cm^{-3} with 416 ± 47 cm^{-3} interstitial particles and 100 ± 9 cm^{-3} droplets, as can be seen in Fig. 4a.

During the event, droplets formed on particles that were 85 nm and larger, i.e., mainly on accumulation mode particles; the highest drop concentration being observed for 168 nm particles (denoted by the blue circles in Fig. 4b). Since accumulation mode particles have a long lifetime if not removed by rain-out or washout, their source region may be southern Sweden as well as the Baltic Sea and northern Germany.

The scavenging ratio (number of cloud droplets divided by the total number concentration, Fig. 4c) shows a steep rise for particles up to 150 nm, while for larger particles the increase is slower. A double-sigmoid was fitted to the data (black line) and the diameter of 50 % activation of 130 nm is indicated (green vertical line). The scavenging ratio is similar to that in event B' in the study by Martinsson et al. (1999) (see Fig. 6 in that publication); the steep rise indicating a higher degree of internally mixed particles and more hygroscopic particles. The slower increase for particles larger than 150 nm may be due to more externally mixed particles with a fraction of less hygroscopic particles that gradually become activated, although the larger size would, on the other hand, favor droplet formation for particles of similar composition.

The size of the ambient cloud interstitial aerosol particles in the cloud in relation to their dry particle size shows a steady increase for the smallest residue sizes, as shown in Fig. 5a. This increase would continue throughout the measured dry particle size range for particles of similar composition, because the interstitial aerosol can be expected to be at equilibrium with the surrounding air. As can be seen in Fig. 5a, the rate of increase in ambient particle size with dry particle size decreases in the region around D_{50} (130 nm). This strongly indicates preferential cloud droplet nucleation scavenging of more hygroscopic particles, whereas the less hygroscopic particles remain as interstitial particles.

The settings of the DMA 2a–f of the DAA are based on dry particle size. Therefore, dry distributions can be obtained directly. To obtain the ambient particle size distribution, a function is fitted to the ambient particle diameter, D_d, as a function of dry (residual) particle diameter, D_p, for each measurement obtained. By differentiating $d \log D_p$ with respect to $d \log D_d$ the function $\frac{d \log D_p}{d \log D_d}$ is obtained and the ambient particle size distribution is calculated from the dry (residual) particle size distribution as follows (Frank et al., 1998):

$$\frac{dN}{d \log D_d} = \frac{dN}{d \log D_p} \frac{d \log D_p}{d \log D_d}. \tag{16}$$

The ambient size distribution obtained (Fig. 5b) is another unique feature of the DAA and shows that interstitial particles below 1 µm are separated from the drop mode by a gap around the ambient particle diameter of 2 µm with a mean ambient particle diameter of 6 µm.

The solute concentration as a function of cloud droplet size can be estimated based on the dry particle volume, measurements of its hygroscopic properties, for example, using a hygroscopic tandem differential mobility analyzer (H-TDMA), and the volume of the cloud droplet. Since we did not have access to H-TDMA data, we assumed approximately constant hygroscopic properties. This study concerns European continental air masses. For such air masses the volume fraction of soluble matter in dry particles of the size range between 0.1 µm and 0.5 µm was approximated to 0.5 ammonium sulfate and 0.5 insoluble material in approximate accordance with Kandler and Schütz (2007). In Fig. 5c it can be seen that the solute concentration depends strongly on the size of the dry (residual) particles. Particle size dependence of the dry particle soluble fraction varies usually much less than ±0.25 (Kandler and Schütz, 2007), i.e. much smaller than the size dependence in the solute concentration, which was based on assumption of a size-independent particle soluble fraction. Limitations in vapor transport by diffusion prevent droplets formed on large particles from increasing in volume at the same relative rate as droplets formed on smaller particles.

5 Conclusions

The DAA was developed specifically for studying the interaction between aerosol particles and cloud/fog droplets. It collects droplets and interstitial particles under ambient conditions and can be used to determine the ambient particle size of individual droplets and the number and sizes of the dry (residual) particles after evaporation of the water. This gives a unique three-parameter data-set (ambient particle diameter, dry (residual) particle diameter and number concentration).

Inversion of DAA data for longterm AIC measurements

M. I. A. Berghof et al.

|◄ | ►|

◄ | ►

Back | Close

Full Screen / Esc

Printer-friendly Version

Interactive Discussion

The DAA inversion approach presented here employs basic corrections to the DAA raw data and different steps to convert the ambient particle charge distributions for certain measured dry particle diameters into an ambient particle size distribution. The components of the DAA, such as the DMAs (dimensions, flows, transfer function) and the CPCs, have been calibrated and characterized to provide the necessary input for data evaluation, ensuring reliable results.

The data can be evaluated with automatic fitting of the charge distribution. For particle number concentration of $dN/d\log D_p = 12.5\,cm^{-3}$ ambient particle diameters down to $0.050\,\mu m$ can be determined with an error of $\pm0.005\,\mu m$. The fitting routine is run automatically, however, manual screening of the results is necessary. In cases of low number concentrations in particular, manual fitting is sometimes needed to identify the interstitial particle and cloud droplet distributions. The estimated uncertainties in the basic DAA parameters, i.e., the diameters of ambient and dry particles and the number concentration and, are 12 %, 6 % and < 13 % respectively.

The inversion algorithm presented here was developed to evaluate long-term DAA data by using a more automated data processing, making it possible to evaluate larger amounts of data. The presented data are part of longterm measurements made during 2010 on Mt. Brocken, performed with a version of the DAA designed for long-term measurements, with better time resolution than the previous version of the instrument. The data show the capability of the DAA when studying the influence of aerosol properties on clouds. The three-parameter DAA dataset is presented in relation to thermodynamic activation with various aspects of the cloud-aerosol data set, such as the number concentration of interstitial particles and cloud droplets, the dry particle size distribution, droplet size distributions, scavenging ratios due to cloud droplet formation and size-dependent solute concentrations. Both the improved version of the DAA and the inversion algorithm will help to relate aerosol and cloud properties to facilitate investigations of cloud and fog formation.

References

Albrecht, B. A.: Aerosols, cloud microphysics, and fractional cloudiness, Science, 245, 1227–1230, 1989. 10270, 10271

Anderson, T. L., Charlson, R. J., and Covert, D. S.: Calibration of a counterflow virtual impactor at aerodynamic diameters from 1 to 15 μm, Aerosol Sci. Tech., 19, 317–329, doi:10.1080/02786829308959639, 1993. 10271

Belyaev, S. and Levin, L.: Techniques for collection of representative aerosol samples, J. Aerosol Sci., 5, 325–338, 1974. 10282

Cederfelt, S. I., Martinsson, B. G., Svenningsson, B., Weidensohler, A., Frank, G., Hansson, H. C., Swietlicki, E., Wendish, M., Beswick, K. M., Bower, K. N., Gallagher, M. W., Pahl, S., Maser, R., and Schell, D.: Field validation of the droplet aerosol analyser, Atmos. Environ., 31, 2657–2670, 1997. 10272, 10276

Draxler, R. and Rolph, G.: HYSPLIT (HYbrid Single-Particle Lagrangian Integrated Trajectory) Model access via NOAA ARL READY Website, available at: http://ready.arl.noaa.gov/HYSPLIT.php (last access: 26 April 2013), NOAA Air Resources Laboratory, Silver Spring, MD, 2013. 10284, 10293

European Environment Agency: Air quality in Europe, 2012 report, Tech. rep., European Environment Agency, 2012. 10284

Frank, G., Martinsson, B. G., Cederfelt, S.-I., Berg, O. H., Swietlick, E., Wendisch, M., Yuskiewicz, B., Heitzenberg, J., Wiedensohler, A., Orsini, D., Stratmann, F., Lai, P., and Ricci, L.: Droplet formation and growth in polluted fogs, Contr. Atmos. Phys., 71, 65–85, 1998. 10272, 10285

Inversion of DAA data for longterm AIC measurements

M. I. A. Berghof et al.

Title Page

Abstract	Introduction
Conclusions	References
Tables	Figures

|◄ | ►|

◄ | ►

Back | Close

Full Screen / Esc

Printer-friendly Version

Interactive Discussion

Frank, G. P., Cederfelt, S.-I., and Martinsson, B. G.: Characterisation of a unipolar charger for droplet aerosols of 0.1–20 µm in diameter, J. Aerosol Sci., 35, 117–134, 2004. 10273, 10278, 10279

Frank, G., Berghof, M., Sjogren, S., and Martinsson, B.: A droplet aerosol analyser (DAA) for longterm aerosol-cloud microphysics measurements, in preparation, 2013. 10273

Kandler, K. and Schütz, L.: Climatology of the average water-soluble volume fraction of atmospheric aerosol, Atmos. Res., 83, 77–92, doi:10.1016/j.atmosres.2006.03.004, 2007. 10286

Karlsson, M. N. A. and Martinsson, B. G.: Methods to measure and predict the transfer function size dependence of individual DMAs, J. Aerosol Sci., 34, 603–625, 2003. 10275

Lawless, P. A.: Particle charging bounds, symmetry rrelation, and an analytic charging rate model for the continuum regime, J. Aerosol Sci., 27, 191–215, 1996. 10278

Liou, K.-N. and Ou, S.-C.: The role of cloud microphysical processes in climate: an assessment from a one-dimensional perspective, J. Geophys. Res., 94, 8599–8607, 1989. 10270

Lohmann, U. and Feichter, J.: Global indirect aerosol effects: a review, Atmos. Chem. Phys., 5, 715–737, doi:10.5194/acp-5-715-2005, 2005. 10270

Martinsson, B. G.: Physical basis for a droplet aerosol analysing method, J. Aerosol Sci., 27, 997–1013, 1996. 10271

Martinsson, B. G., Cederfelt, S. I., Svenningsson, B., Frank, G., Hansson, H. C., Swietlicki, E., Wiedensohler, A., Wendisch, M., Gallagher, M. W., Colvile, R. N., Beswick, K. M., Choularton, T. W., and Bower, K. N.: Experimental determination of the connection between cloud droplet size and its dry residue size, Atmos. Environ., 31, 2477–2490, 1997. 10272

Martinsson, B. G., Frank, G. P., Cederfelt, S.-I., Swietlicki, E., Berg, O. H., Zhou, J., Bower, K. N., Bradbury, C., Birmili, W., Stratmann, F., Wendisch, M., Wiedensohler, A., and Yuskiewicz, B. A.: Droplet nucleation and growth in orographic clouds in relation to the aerosol population, Atmos. Res., 50, 289–315, 1999. 10272, 10285

Martinsson, B. G., Frank, G., Cederfelt, S. I., Berg, O. H., Mentes, B., Papaspiropolos, G., Swietlicki, E., Zhou, J., Flynn, M., Bower, K. N., Choularton, T. W., Mäkelä, J., Virkkula, A., and v. Dingenen, R.: Validation of very high cloud droplet number concentrations in air masses transported thousands of kilometres over the ocean, Tellus, 52, 801–814, 2000. 10272

Martinsson, B. G., Karlsson, M. N. A., and Frank, G.: Metodology to estimate the transfer function of individual differential mobility analyzers, Aerosol Sci. Tech., 35, 815–823, 2001. 10275

Title Page

Abstract | Introduction

Conclusions | References

Tables | Figures

|◄ | ►|

◄ | ►

Back | Close

Full Screen / Esc

Printer-friendly Version

Interactive Discussion

Noone, K. J., Ogren, J. A., Heintzenberg, J., Charlson, R. J., and Covert, D. S.: Design and calibration of a counterflow virtual impactor for sampling of atmospheric fog and cloud droplets, Aerosol Sci. Tech., 8, 235–244, doi:10.1080/02786828808959186, 1988. 10271

Ogren, J. A., Heintzenberg, J., and Charlson, R. J.: In-situ sampling of clouds with a droplet to aerosol converter, Geophys. Res. Lett., 12, 121–124, doi:10.1029/GL012i003p00121, 1985. 10271

Sjogren, S., Frank, G. P., Berghof, M. I. A., and Martinsson, B. G.: Continuous stand-alone controllable aerosol/cloud droplet dryer for atmospheric sampling, Atmos. Meas. Tech., 6, 349–357, doi:10.5194/amt-6-349-2013, 2013. 10273

Slowik, J. G., Cziczo, D. J., and Abbatt, J. P. D.: Analysis of cloud condensation nuclei composition and growth kinetics using a pumped counterflow virtual impactor and aerosol mass spectrometer, Atmos. Meas. Tech., 4, 1677–1688, doi:10.5194/amt-4-1677-2011, 2011. 10271

Sorensen, C. M., Gebhart, J., O'Hern, T. J., and Rader, D. J.: Optical Measurement Techniques: Fundamentals and Applications, John Wiley & Sons, Inc., 269–312, doi:10.1002/9781118001684.ch13, 2011. 10271

Spiegel, J. K., Zieger, P., Bukowiecki, N., Hammer, E., Weingartner, E., and Eugster, W.: Evaluating the capabilities and uncertainties of droplet measurements for the fog droplet spectrometer (FM-100), Atmos. Meas. Tech., 5, 2237–2260, doi:10.5194/amt-5-2237-2012, 2012. 10271

Stevens, B. and Feingold, G.: Untangling aerosol effects on clouds and precipitation in a buffered system, Nature, 461, 607–613, 2009. 10271

Stolzenburg, M. R.: An ultrafine aerosol size distribution measuring system., Ph.D. thesis, University of Minnesota, 1988. 10275

Twomey, S.: Pollution and the planetary albedo, Atmos. Environ., 8, 1251–1256, 1974. 10270

Warner, J.: A reduction in rainfall associated with smoke from sugar-cane fires – an inadvertent weather modification?, J. Appl. Meteorol., 7, 247–251, 1968. 10270

Wiedensohler, A.: An approximation of the bipolar charge distribution for particles in the submicron size range, J. Aerosol Sci., 19, 387–389, 1988. 10276

Title Page

Abstract | Introduction

Conclusions | References

Tables | Figures

◀ | ▶

◀ | ▶

Back | Close

Full Screen / Esc

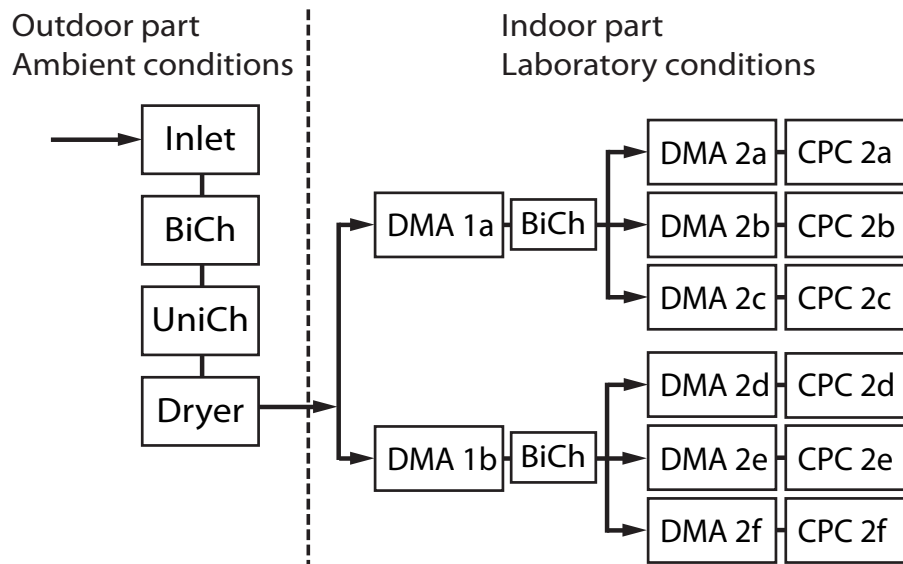Printer-friendly Version

Interactive Discussion

Fig. 1. The principle of the DAA. Droplets and particles are processed in several steps by aerosol charging mechanisms in bipolar (BiCh) and unipolar chargers (UniCh), diffusion drying (Dryer), electrostatic aerosol spectrometry (DMA), and counting in condensation particle counters (CPC) in order to obtain the desired relationships.
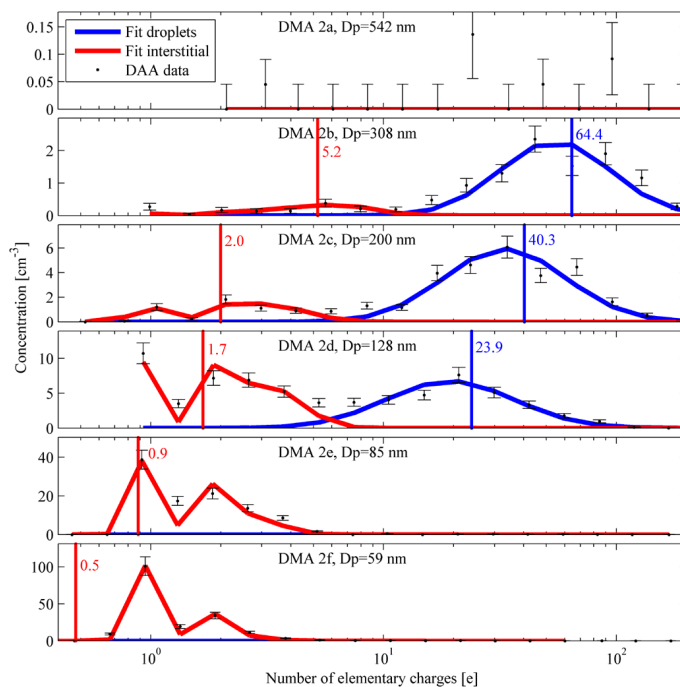
Fig. 2. Example of results obtained from data collected at Mt. Brocken, one run from 31 August 2010 00:53–01:03 UTC. The panels show charge distribution data from the DMA 2a–f, including the standard error for Poisson counting of the raw counts. In this example one or two fits were performed for each DMA 2a–f, which can be classified as interstitial particles and droplets. In the top panel, showing the results from DMA 2a for the largest dry particle diameter measured in this run, and in the two lowest panels, showing the results for the two samllest dry particle diameters measures (DMA 2e and 2f) there were insufficient particles and droplets to allow a fit. Note the varying scale on the *y* axes.

Title Page

Abstract | Introduction

Conclusions | References

Tables | Figures

|◄ | ►|

◄ | ►

Back | Close

Full Screen / Esc

Printer-friendly Version

Interactive Discussion

(a)

(b)
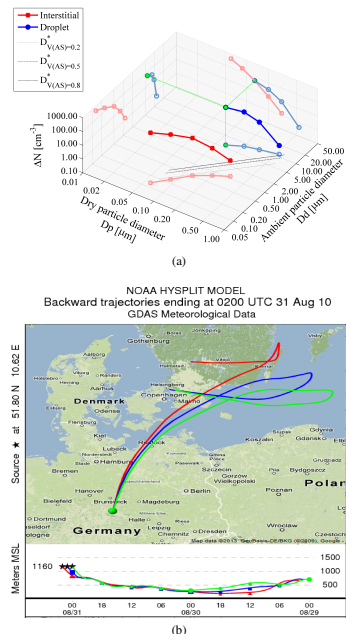
Fig. 3. (a) Concentration in each measured size interval ΔN of droplets and residual particles as a function of ambient particle and dry particle diameter on 31 August 2010, 23:51 UTC. The three black lines in the $D_p - D_d$ plane indicate the the critical diameter of activation according to Köhler's theory for different volume fractions of ammonium sulfate in the particles, $D^*_{V(AS)}$. The projections in paler colors show the distribution of ambient particles (left, $D_d - \Delta N$ plane), the distribution of dry (residual) particles (right, $D_p - \Delta N$ plane) and ambient particle diameter D_d as a function of dry (residual) particle diameter D_p (bottom, $D_p - D_d$ plane). **(b)** The 48 h back trajectories arriving at Mt. Brocken at 30 August 2010, 23:00 UTC (green), 31 August 2010, 01:00 UTC (blue) and 02:00 UTC (red), derived with the HYSPLIT model are shown. The HYSPLIT trajectories arrive at 1161 m above sea-level, representing 20 m above the station at the summit of Mt. Brocken (Draxler and Rolph, 2013).

Full Screen / Esc

Printer-friendly Version
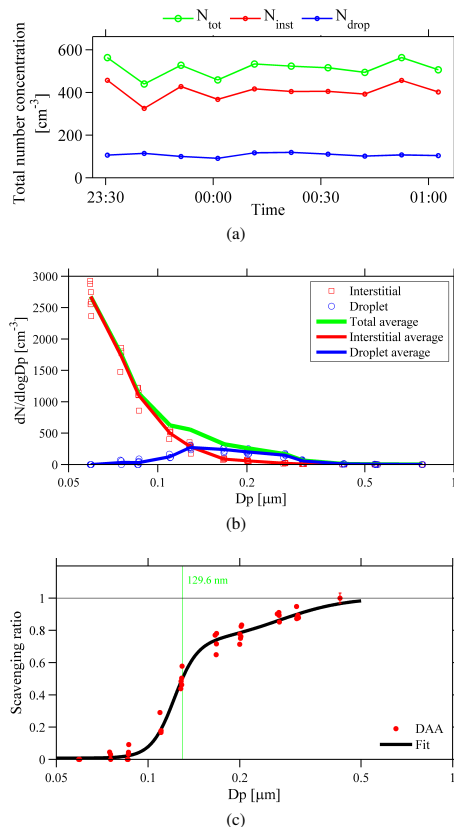
Interactive Discussion

Fig. 4. (a) The total, interstitial and droplet number concentrations during the event, in the size range 49 to 563 nm. **(b)** Dry (residual) particle size distribution, $dN/d\log D_p$, of interstitial particles and droplets including averages (lines). **(c)** DAA scavenging ratio during the cloud event (red dots) with error-bars indicating the estimated standard deviation in DAA counts during the event (smaller than the marker size for almost all data points), and a log-normal double-sigmoid fit (black line). The diameter for 50 % activation is 0.13 µm, indicated by the green line.
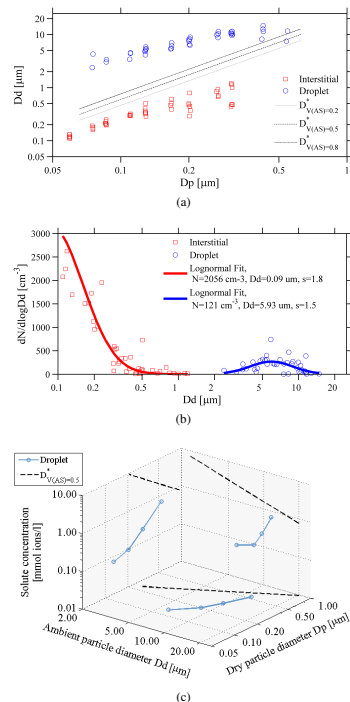
Fig. 5. (a) Ambient particle diameter, D_d, as a function of dry (residual) diameter, D_p, during the event. The three black lines show the critical diameter of activation $D^*_{V(AS)}$ for different volume fractions of ammonium sulfate in the particles. **(b)** Ambient particle size distribution, $dN/d\log D_d$, for interstitial particles and droplets during the event. The bold lines are log-normal fits to the data. **(c)** Estimated cloud droplet solute concentration as a function of the droplet size and dry (residue) particle size on 30 August 2010, at 23:51 UTC. The projections show droplet solute concentration as a function of interstitial particle diameter (left) and ambient particle diameter (right). The bottom projection shows the ambient particle diameter, D_d, as a function of dry (residual) particle diameter D_p. The dashed lines show the limits of droplet activation for an ammonium sulfate volume fraction of 0.5, according to the Köhler theory in each projection.